J. Fluid Mech. (1993), *vol.* 247, *pp.* 65–77

Copyright © 1993 Cambridge University Press

On some kinematic versus dynamic properties of homogeneous turbulence

By L. SHTILMAN, M. SPECTOR AND A. TSINOBER
Department of Fluid Mechanics and Heat Transfer, Tel-Aviv University, Ramat Aviv, Tel-Aviv, 69978, Israel

(Received 13 June 1991 and in revised form 29 June 1992)

A comparison is made between a number of properties of a quasi-homogeneous isotropic turbulent field obtained from a direct numerical simulation of the Navier–Stokes equation and its random counterpart with the same energy spectrum. It is demonstrated that some effects in a real flow have a considerable contribution of a kinematic nature (e.g. reduction of nonlinearity), while others are mostly dynamical (e.g. alignment between vorticity and eigenvectors of the rate of strain).

1. Introduction

Turbulent flows are believed to be governed by the Navier–Stokes equations. On the other hand one of the basic features of turbulent flows is their (apparent) randomness or stochasticity. This last property is considered to be a direct consequence of the nature of attractors of Navier–Stokes equations (e.g. Landau & Lifshitz 1987, pp. 108–129; Monin 1986; George 1990; Frisch & Orszag 1990) at high Reynolds number. It is natural to ask what are the differences between turbulent flows and other chaotic phenomena such as kinematic (Lagrangian) chaos (Aref 1990) or simply random Gaussian processes. The importance of this question is two-fold. From the basic point of view it is of interest since most theories (models) do not make a direct appeals the Navier–Stokes equations, e.g. the most popular $k^{-\frac{5}{3}}$ theories or a variety models of intermittency (Hosokawa 1990; Sreenivasan 1991 and references therein). Secondly, the question is of importance in the context of kinematical simulations of turbulent flows for various practical purposes (Fung *et al.* 1992 and references therein).

There is much in common between turbulent flow fields and Gaussian random processes, e.g. the one-point distribution of the velocity field is nearly Gaussian. However, the velocity derivatives, etc. appear to be essentially different from Gaussian, e.g. the prevalence of exponential probability density distributions (Narasimha 1990; Gagne 1991 and references therein). Therefore, comparing real turbulent flows with the Gaussian counterparts may be extremely useful in elucidating the characteristic dynamic properties of Navier–Stokes turbulence versus those – we call them kinematic – which are common to both Navier–Stokes turbulence and its Gaussian counterpart. Kraichnan & Panda (1988) started this kind of comparison and showed that the mean square of the total nonlinear term in homogeneous Navier–Stokes equation turbulence is 0.57 of its Gaussian counterpart and Chen *et al.* (1989) have shown that this reduction happened mostly in the high-wavenumber region of the spectrum (see also Herring & Kerr 1989). Shtilman & Polifke (1989) have shown that the Lamb vector (vorticity velocity cross-product) contains a large potential part. It appears that the kinematics has a large

contribution to this effect, since this is also a property of a random Gaussian solenoidal field (Shtilman & Polifke 1989; Tsinober 1990 and see below).

It has been found recently that there exist several alignments in homogeneous turbulence. Ashurst *et al.* (1987*b*) discovered the alignment of vorticity ω_i with the eigenvectors e_j^k of the rate-of-strain tensor S_{ij}, especially with the intermediate one. Ashurst *et al.* (1987*a*) have also found that the gradient of the pressure exhibits a tendency to align with the largest compressive eigenvector of the rate-of-strain tensor. Several authors have found some tendency for alignment of vorticity ω_i and velocity u_i vectors (e.g. Shtilman, Pelz & Tsinober 1988 and references therein; Herring & Métais 1989; Polifke 1991); Shtilman & Polifke (1989) found a strong tendency for alignment between the Lamb vector $\lambda_i = \epsilon_{ijk}\omega_j u_k$ and its potential part; finally Tsinober, Kit & Dracos (1991, 1992) introduced an angle between vorticity and the vortex stretching vector $W_i = \omega_j S_{ij}$ which appeared to have a strong tendency for alignment in the strict sense. Though it is tempting to consider the above alignments as a manifestation of coherence, i.e. to see the alignments as purely dynamical effects, it will be shown below that some of them are mostly of a kinematic nature.

This note is an attempt to get an idea about the contribution of kinematical and dynamical effects to some of the observed properties of quasi-homogeneous and isotropic turbulent flows. This has been done via comparison of these for two fields: one obtained from direct numerical simulations and the other one being its random counterpart with the same energy spectrum or with analytical calculations for a random Gaussian field.

2. Results

We have used the data of Polifke & Shtilman (1989) from direct numerical simulations of the incompressible Navier–Stokes equation together with those obtained from a random counterpart of the Navier–Stokes equation simulation. These simulations are based on a pseudospectral code with resolution $64 \times 64 \times 64$ and details of simulations as well as the procedure for creation of the random counterpart are given in Appendix A. The details of theoretical calculations covering the calculation of probability density functions of several quantities, like ω^2, $\omega_i S_{ij} \omega_j$, etc. for a solenoidal Gaussian field are given in Appendix B.

2.1. *Dissipation, enstrophy and enstrophy generation*

First we note that the $y^{-\frac{1}{2}}$ singularity in the P_4 probability distribution function (PDF), for example of $(\partial u_1/\partial x_1)^2$, is a purely kinematic effect as can be seen from (B 16). It is noteworthy that PDFs for dissipation and enstrophy of a Gaussian field do not have the singularity and are different, as is seen from (B 14) (B 15). In figure 1 we present all three PDFs for a Gaussian field. These PDFs from Navier–Stokes simulations are shown in figure 2 and exhibit very similar behaviour. In particular the PDFs show that there is a greater probability of finding very small or very large values of enstrophy than the corresponding values of dissipation, implying that kinematical effects can made a greater contribution to stronger intermittency of vorticity than of dissipation. A simple demonstration of the difference between a random field and the Navier–Stokes simulated one is seen on the histograms in figure 3(*a*, *b*) where enstrophy is plotted versus dissipation and vice versa for the Navier–Stokes simulated field. The same plots for a random field are just flat as also follows from calculations for a Gaussian field (see Appendix B). The PDF of the

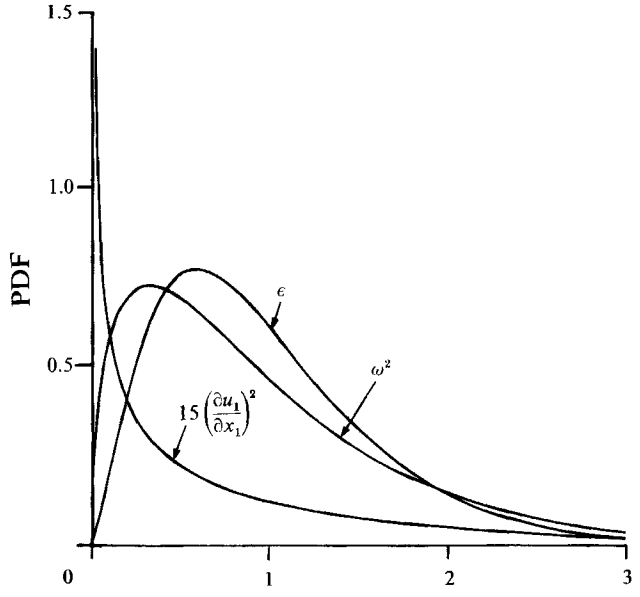

FIGURE 1. Normalized PDFs of $15(\partial u_1/\partial x_1)^2$, $\frac{1}{2}\omega^2$ and dissipation $S_{ij}S_{ij}$ for a Gaussian velocity vector field.

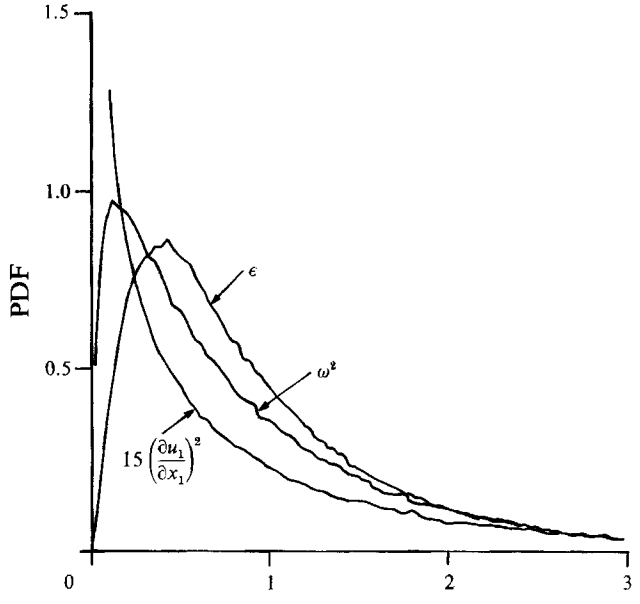

FIGURE 2. Same as figure 1 for Navier–Stokes simulation.

enstrophy generation $\omega_i\omega_j S_{ij}$ are shown in figure 4. The essential difference is that the PDF for the Navier–Stokes simulated field is not symmetric as a result of a net positive enstrophy generation. This last effect can be seen much better in figure 5 showing the PDF of the cosine of the angle between vorticity ω_i and the vortex stretching vector $W_i = \omega_j S_{ij}$. One can easily observe the essential difference between the Navier–Stokes simulated case and the Gaussian one calculated from (B 19).

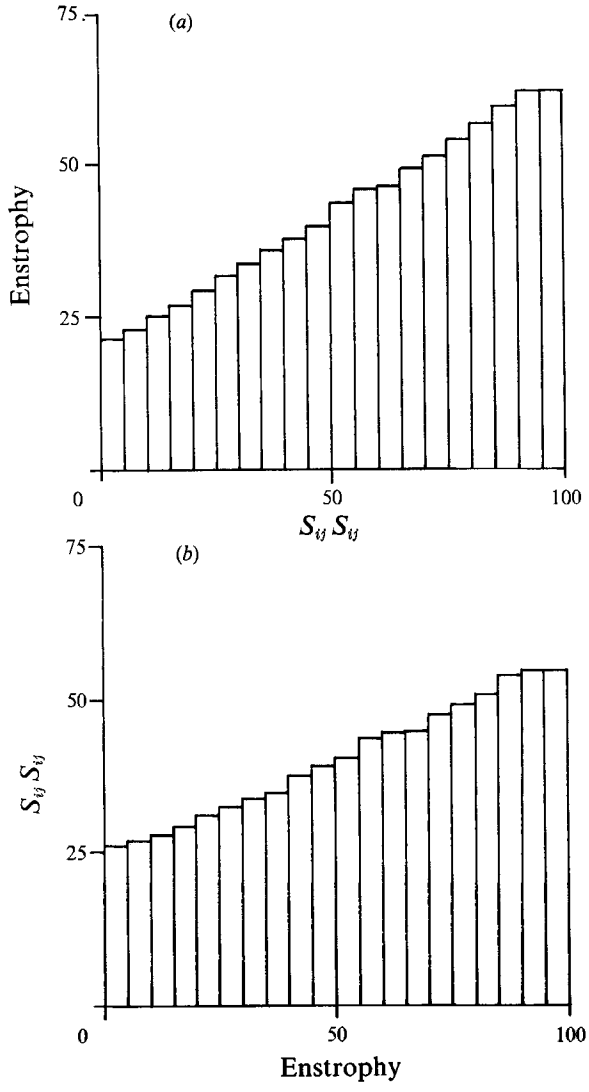

FIGURE 3. Histogram of (*a*) enstrophy versus dissipation and (*b*) vice versa for Navier–Stokes simulation.

Qualitatively similar results have been obtained in laboratory experiments by Tsinober *et al.* (1991). We conclude that strict alignment between ω and W is an essentially dynamical effect. A histogram of enstrophy versus enstrophy generation for the Navier–Stokes simulated case (figure 6) again shows a qualitative difference with the case of a random field in which the histogram is flat. The plot is skewed to the left as a result of a net positive enstrophy generation.

2.2. *Alignments of vorticity and pressure gradient with eigenvectors of the rate-of-strain tensor*

It is straightforward to show that the PDFs of the cosine of the angle between vorticity and the eigenvectors of the strain-rate tensor for the Gaussian field are flat (see Appendix B). The same is true for the random counterpart field. One easily

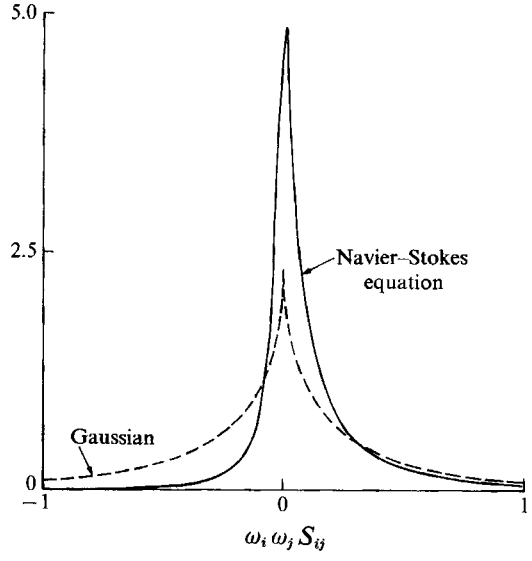

FIGURE 4. PDFs of enstrophy generation: Navier–Stokes simulation compared to Gaussian field.

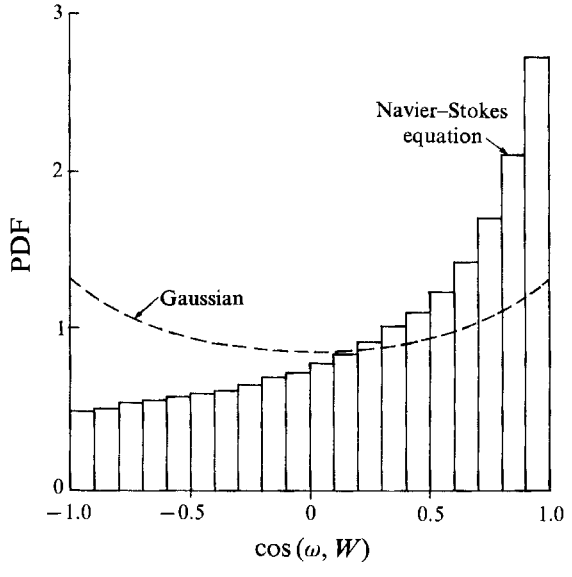

FIGURE 5. PDFs of the cosine of the angle between vorticity and the vortex stretching vector: Navier–Stokes simulation compared to Gaussian field.

concludes that these kind of alignments are essentially dynamical effects. Similarly the alignment between the pressure gradient and the eigenvectors of the rate-of-strain tensor is a dynamical effect too. We obtained the same results for these alignments as Ashurst *et al.* (1987*a*, *b*), She, Jackson & Orszag (1990) and Vincent & Meneguzzi (1991). The most prominent is the strong tendency for alignment between vorticity and the intermediate eigenvector of the rate-of-strain tensor.

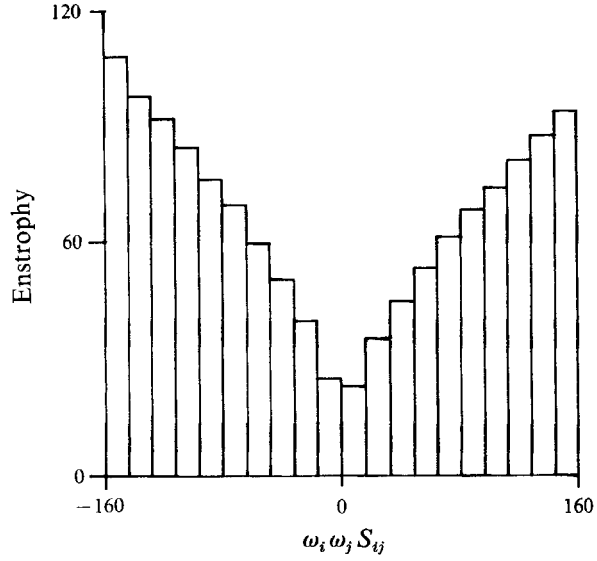

FIGURE 6. Histogram of enstrophy versus enstrophy generation for a Navier–Stokes simulation.

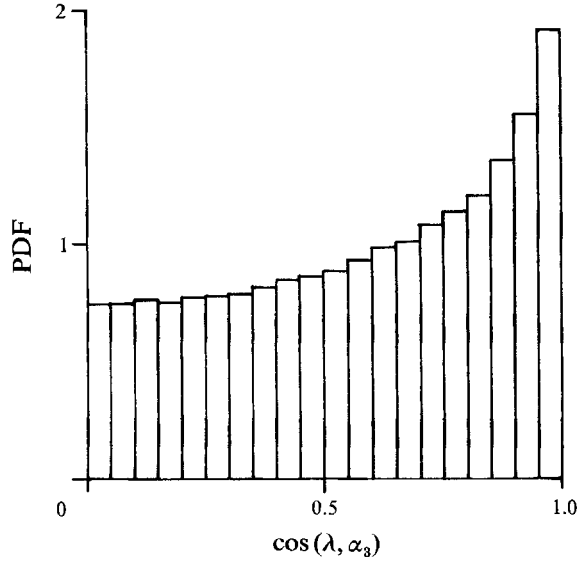

FIGURE 7. PDF of the cosine of the angle between the Lamb vector and the largest compressive rate of strain α_3.

2.3. *Alignments of the Lamb vector $\omega \times v$, pressure gradient and the eigenvectors of the rate-of-strain tensor*

There is a tendency of alignment between the Lamb vector and the largest compressive strain for the Navier–Stokes simulated field. It is for this reason that the velocity vector is mostly located in the plane formed by two other eigenvectors (She *et al.* 1990). However, the conclusion that the results shown in figure 7 (for the Navier–Stokes simulated case) provide a dynamical explanation of the reduction of nonlinearity, i.e. reduction of the solenoidal part of Lamb vector, is not completely true for the following reason. Let us look at the PDF of the cosine of the angle

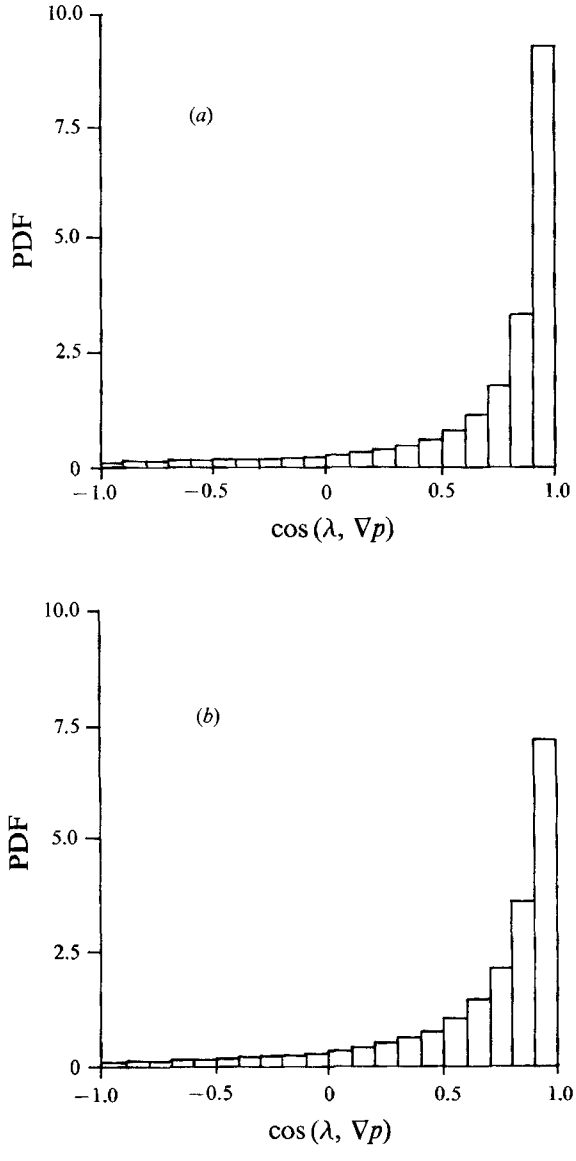

FIGURE 8. PDF of the cosine of the angle between the Lamb vector and its potential part (i.e. pressure gradient): (*a*) Navier–Stokes simulation, (*b*) Gaussian (random counterpart).

between the Lamb vector and its potential part, which is identical to the pressure gradient for the case of homogeneous flow (figure 8). One can see from figure 8 that most of the alignment between the two is a purely kinematic effect – though in the real flow it is somewhat stronger.

2.4. *Alignment between velocity and vorticity*

The effect is purely dynamical since the PDF of the cosine of the angle between velocity and vorticity is flat for a Gaussian field as well as for the random counterpart field.

3. Concluding remarks

Among the properties of homogeneous turbulent flows there are some that have a considerable contribution of a kinematic nature, i.e. very similar to those of random Gaussian fields. One prominent example is the alignment between the Lamb vector and the pressure gradient leading to considerable reduction of nonlinearity. On the other hand enstrophy generation and alignment between vorticity and the eigenvectors of the rate of strain are essentially dynamical effects which are not present in random Gaussian fields at all. The comparison made above indicates that kinematical effects can be important for the dynamics of turbulent flows and that care is necessary to distinguish between the two.

We would like to thank Dr Y. Murakami for his help in developing the numerical procedure used in the creation of random fields. This work was performed under partial support of US Department of Energy Grant No. DE-FG0288ER13837. All computations were performed at Lawrence Livermore National Laboratory.

Appendix A

The Navier–Stokes equation has been solved by a pseudospectral method. The periodic boundary conditions and the slave-frog second-order scheme have been used for the time stepping. The resolution $N = 64^3$ and the octapentagonal dealiasing method was adopted. The initial spectrum was narrow banded. We have used a field obtained from forced turbulence simulations similar to those made by Shtilman & Polifke (1989) for decaying turbulence. The forcing in k-space is δ-correlated and has a k^{-5} envelope. This field corresponds to a statistically steady state of the numerical turbulence with $\nu = 0.015$ and a time-independent and spatially random forcing exerted at large scales ($3 < k < 4$) at each step. The field was obtained after around six turnover times (1000 time steps with $\Delta t = 0.004$) thus assuring independence of initial conditions. The helicity injected by force has not been controlled since it has been shown by Polifke (1991) that only a very high (actually artificial) level of helicity will affect the flow. The characteristic parameters of the turbulent field are: total energy $E(t) = 1.29$, total enstrophy $\Omega(t) = 35.0$, mean helicity $H(t) = 0.79$, the Taylor microscale Reynolds number, $R_\lambda = (\frac{10}{3})^{\frac{1}{2}} E(t)/[\nu(\Omega(t))^{\frac{1}{2}}] = 26.5$, turnover time $\tau = (\frac{3}{4}\pi \int k^{-1} E(k)\,\mathrm{d}k/(\frac{2}{3}E)^{\frac{1}{2}} = 0.7$, the skewness of the x-derivative of the u-component $S = -\langle(\partial u/\partial x)^3\rangle/(\langle(\partial u/\partial x)^2\rangle)^{\frac{3}{2}} = 0.52$, and the flatness of the x-derivative of the u-component $F = \langle(\partial u/\partial x)^4\rangle/\langle(\partial u/\partial x)^2\rangle^2 = 4.2$. All scales have been fully resolved.

The random field that we have used for comparison with the results of the direct numerical simulations have the same energy and helicity spectra as the original field. The field was generated in the following way. As a result of incompressibility, $\boldsymbol{k}\cdot\mathrm{Re}\,\boldsymbol{v}(\boldsymbol{k}) = \boldsymbol{k}\cdot\mathrm{Im}\,\boldsymbol{v}(\boldsymbol{k}) = 0$, where $\mathrm{Re}\,\boldsymbol{v}(\boldsymbol{k})$ and $\mathrm{Im}\,\boldsymbol{v}(\boldsymbol{k})$ are, respectively, the real and the imaginary parts of the velocity field in Fourier space. Thus we have four degrees of freedom for each mode. The energy conservation law leads to $E(\boldsymbol{k}) = \frac{1}{2}|\boldsymbol{v}(\boldsymbol{k})|^2 = \frac{1}{2}[(\mathrm{Re}\,\boldsymbol{v}(\boldsymbol{k}))^2 + (\mathrm{Im}\,\boldsymbol{v}(\boldsymbol{k}))^2] = \text{constant}$ (i.e. $E'(\boldsymbol{k}) = E(\boldsymbol{k})$). This restriction reduces the number of degrees of freedom to three, essentially three phases, that can be varied at will, while $|\boldsymbol{v}(\boldsymbol{k})|$ is invariant. We also conserve the helicity spectra, i.e. we preserve the angle $\phi(\boldsymbol{k})$ between the real and imaginary parts of $\boldsymbol{v}(\boldsymbol{k})$, but rotate this pair in a uniformly random way in all directions [0–2π] in the plane perpendicular to the vector $\boldsymbol{k}$. Clearly this procedure preserves both energy $E(\boldsymbol{k})$ and

helicity $H(\boldsymbol{k})$. More details on the matching of helicity and energy spectra of a random field with those from numerical simulations can be found in Murakami, Shtilman & Levich (1992).

Appendix B

We consider probability distribution functions (PDFs) of some quantities depending on the velocity and its derivatives under the assumption that the velocity field is random homogeneous isotropic and Gaussian. The latter means that the probability density of some configuration v_k is

$$Q\{v_k\} \sim \exp\left\{-\frac{1}{2}\int \mathrm{d}^3 k T_{\beta\beta'}(k)\, v_{\beta_k} v^*_{\beta'_k}\right\}, \tag{B 1}$$

where v_{β_k} is the Fourier amplitude of the βth velocity component and $v^*_{\beta_k} = v_{\beta_{-k}}$.

It is well known that for a homogeneous and isotropic field the matrix $T_{\beta\beta'}$ has the following form:

$$T_{\beta\beta'}(k) = \frac{2}{G(k)}\left(\delta_{\beta\beta'} - \frac{k_\beta k_{\beta'}}{k^2}\right) + \frac{1}{\mu(k)}\frac{k_\beta k_{\beta'}}{k^2}. \tag{B 2}$$

The inverse matrix $T^{-1}_{\beta\beta'}$ defines the spectral density of the field $\boldsymbol{v}$:

$$\begin{aligned} \langle v_{\beta_k} v^*_{\beta'_{k'}}\rangle &= T^{-1}_{\beta\beta'}(\boldsymbol{k})\,\delta(k-k'), \\ T^{-1}_{\beta\beta'}(\boldsymbol{k}) &= \tfrac{1}{2}G(k)\left(\delta_{\beta\beta'} - \frac{k_\beta k_{\beta'}}{k^2}\right) + \mu(k)\frac{k_\beta k_{\beta'}}{k^2}. \end{aligned} \tag{B 3}$$

To avoid dealing with singular matrices we introduced a longitudinal correlator $\mu(k)$ as well. For incompressible flow $\mu(k)$ will be put equal to zero. The spectral density of $\boldsymbol{\omega} = \boldsymbol{\nabla}\times\boldsymbol{v}$ and $\theta = \boldsymbol{\nabla}\cdot\boldsymbol{v}$ can be written:

$$\langle \omega_{\beta_k}\omega_{\beta'_{k'}}\rangle = \tfrac{1}{2}k^2 G(k)\left(\delta_{\beta\beta'} - \frac{k_\beta k_{\beta'}}{k^2}\right)\delta(k+k'), \quad \langle \theta_k \theta_{k'}\rangle = \mu(k)\,\delta(k+k'),$$

so that

$$\langle v^2\rangle = \int \mathrm{d}^3 k (G(k)+\mu(k)); \quad \langle \omega^2\rangle = \int k^2 G(k)\,\mathrm{d}^3 k; \quad \langle \theta^2\rangle = \int k^2 \mu(k)\,\mathrm{d}^3 k.$$

In order to find the joint PDF for some set of L quantities

$$y^{(n)} = \int b^{(n)}_\beta(k)\, v_{\beta_k}\,\mathrm{d}k \tag{B 4}$$

which are linear in v, one has to calculate to following functional integral

$$P\{y^n\} = \int \mathrm{D}v_k\, Q \prod_{n=1}^{L} \delta\left(y^{(n)} - \int b^{(n)}_{\beta_k} v_{\beta_k}\,\mathrm{d}^3 k\right)\left(\int \mathrm{D}v_k\, Q\right)^{-1},$$

where Q is defined in (B 1).

Using the standard representation for a δ-function, $\delta(y) = (1/2\pi)\int \mathrm{d}q\, \mathrm{e}^{\mathrm{i}qy}$, one can rewrite $P\{y^n\}$ in the following form:

$$P\{y^n\} = \frac{1}{(2\pi)^L}\int \prod \mathrm{d}q\, \mathrm{e}^{\mathrm{i}q_n y^n} \int \mathrm{D}v_k \exp\{-F\}\left(\int \mathrm{D}v_k\, Q\right)^{-1}, \tag{B 5}$$

where

$$F = \int \mathrm{d}^3k(\tfrac{1}{2}T_{\beta\beta'}(k)\, v_{\beta_k} v^*_{\beta'_k} + \mathrm{i}q_n\, b^n_\beta(k)\, v_{\beta_k}). \tag{B 6}$$

The functional integral in (B 5) can be calculated in the same way as is done for usual Gaussian integrals. This is done by shifting the variables of integration

$$v_{\beta_k} = v^{(0)}_{\beta_k} + u_{\beta_k},$$

where $v^{(0)}_{\beta_k}$ define the extremal of functional F:

$$T_{\beta\beta'} v^{(0)}_{\beta'_k} + \mathrm{i}q_n\, b^n_\beta(k) = 0.$$

In this way the terms linear in u_{β_k} are eliminated and the functional F takes the following form:

$$F = \frac{1}{2}\int \mathrm{d}^3k T_{\beta\beta'}\, u^*_{\beta_k} u_{\beta'_k} - \tfrac{1}{2}q_n\, q_m \int T^{-1}_{\beta\beta'}\, b^{*n}_\beta\, b^m_{\beta'_k}\, \mathrm{d}^3k.$$

Subsequent functional integration in (B 5) with respect to variables u_{β_k} gives a factor which is exactly cancelled by denominator in (B 5) resulting in the following expression for the PDF:

$$P\{y^n\} = \frac{1}{(2\pi)^L}\int \prod \mathrm{d}q \exp\{\mathrm{i}q_n\, y^n - \tfrac{1}{2}q_n\, q_m A_{nm}\}, \tag{B 7}$$

where

$$A_{nm} = \int \mathrm{d}^3k T^{-1}_{\beta\beta'}(k)\, b^{*n}_\beta(k)\, b^m_{\beta'}(k). \tag{B 8}$$

So, to find the joint PDF for the set of quantities y^n, linearly depending on v, one has to determine the coefficients $b^n_\beta(k)$ in (B 4) to find the matrix A_{mn} using the correlation function $\boldsymbol{T}^{-1}$ (B 3) and to calculate the integral (B 7) which is Gaussian again (note that the latter is a usual, i.e. non-functional, integral).

We start now with the calculation of the joint PDF of vorticity components

$$\omega_\gamma(x_0) = e_{\alpha\beta\gamma}\frac{\partial v_\beta}{\partial x_\alpha}(x_0)$$

and the components of the rate-of-strain tensor $S_{ik} = (\partial v_i/\partial x_k) + (\partial v_k/\partial x_i)$. It is convenient to introduce the following quantities as independent variables characterizing the matrix $\hat{\boldsymbol{S}}$:

$$s_1 = S_{23}, \quad s_2 = S_{13}, \quad s_3 = S_{12}, \quad \text{the trace}\,\theta = \tfrac{1}{2}S_{ii} \equiv \operatorname{div} \boldsymbol{v}$$

and another two combinations of diagonal matrix elements 'orthogonal' to θ:

$$s_4 = \tfrac{1}{2}(S_{11} - S_{22}), \quad s_5 = \frac{1}{2\sqrt{3}}(S_{11} + S_{22} - 2S_{33}),$$

so that the dissipation is

$$\epsilon = \tfrac{1}{2}S_{ij}S_{ij} = \sum_1^5 s_i^2 + \tfrac{2}{3}\theta^2. \tag{B 9}$$

The corresponding values of $b^n_\beta(k)$ $(n = 1, 2, \ldots, 9)$ in (B 4) are given by

$$b^{(\omega_\alpha)}_\beta(k) = \mathrm{i}k_\gamma e_{\gamma\beta\alpha}\,\mathrm{e}^{\mathrm{i}\boldsymbol{k}\cdot\boldsymbol{r}_0}, \quad b^{(s_\alpha)}_\beta(k) = \mathrm{i}(k_{\alpha_2}\delta_{\beta\alpha_1} + k_{\alpha_1}\delta_{\beta\alpha_2})\,\mathrm{e}^{\mathrm{i}\boldsymbol{k}\cdot\boldsymbol{r}_0}.$$

Here $\alpha = 1, 2, 3$ and α_1, α_2 are indices complementary to α,

$$b^{(s_4)}_\beta(k) = \mathrm{i}(k_x\delta_{1\beta} + k_y\delta_{2\beta})\,\mathrm{e}^{\mathrm{i}\boldsymbol{k}.\boldsymbol{r}_0}, \quad b^{(s_5)}_\beta(k) = \frac{\mathrm{i}}{\sqrt{3}}(k_x\delta_{1\beta} + k_y\delta_{2\beta} - 2k_z\delta_{3\beta})\,\mathrm{e}^{\mathrm{i}\boldsymbol{k}.\boldsymbol{r}_0}$$

and $b_\beta^{(\theta)}(k) = \mathrm{i}k_\beta \mathrm{e}^{\mathrm{i}k.r_0}$. The subsequent calculation of the matrix A_{mn} shows that it is diagonal, resulting in factorization of the joint PDF

$$P_9(\omega_a, s_i, \theta) = P_1(\theta) P_5(s_i) P_3(\omega_i),$$

where

$$P_1(\theta) = (2\pi\langle\theta^2\rangle)^{-\frac{1}{2}} \exp\left(-\frac{1}{2}\frac{\theta^2}{\langle\theta^2\rangle}\right) \tag{B 10}$$

(remembering that $\theta = \operatorname{div} \boldsymbol{v} = \frac{1}{2}\mathrm{Tr}\,\hat{\boldsymbol{S}}$),

$$P_5(s_i) = [2\pi(\tfrac{1}{5}\langle\omega^2\rangle + \tfrac{4}{15}\langle\theta^2\rangle)]^{-\frac{5}{2}} \exp\{-\tfrac{1}{2}(\textstyle\sum s_i^2)/(\tfrac{1}{5}\langle\omega^2\rangle + \tfrac{4}{15}\langle\theta^2\rangle)\}, \tag{B 11}$$

$$P_3(\omega_i) = \left[2\pi\frac{\langle\omega^2\rangle}{3}\right]^{-\frac{3}{2}} \exp\{-\tfrac{1}{2}\textstyle\sum\omega_i^2/(\frac{1}{3}\langle\omega^2\rangle)\}. \tag{B 12}$$

In the same way it can be shown that the velocity field with the PDF

$$P(v_i) = \left(2\pi\frac{\langle v^2\rangle}{3}\right)^{-\frac{3}{2}} \exp\{-\tfrac{1}{2}\textstyle\sum v_i^2/(\frac{1}{3}\langle v^2\rangle)\} \tag{B 13}$$

does not correlate either with vorticity ω_i or with S_{ij}. Note that this is true only for one-point PDFs. If different spatial points are considered the correlations between v_i, ω_i and S_{ij} generally do not vanish. Now we shall consider only incompressible flows

$$\operatorname{div} \boldsymbol{v} \equiv 0, \quad \langle\theta^2\rangle = 0, \quad \text{so that } P_1(\theta) = \delta(\theta)$$

and the dispersion in the PDF P_5 (B 13) reduces simply to $\frac{1}{5}\langle\omega^2\rangle$. The PDF for enstrophy ω^2 and dissipation ϵ can now be obtained by integration of (B 11) and (B 12) over spatial angles in five-dimensional (for ϵ) and three-dimensional (for ω^2) space, resulting in

$$P(\epsilon = y) = \frac{1}{(2\pi)^{\frac{1}{2}}}\frac{1}{3}\left(\frac{5}{\langle\omega^2\rangle}\right)^{\frac{5}{2}} y^{\frac{3}{2}} \exp\left(-\frac{5}{2}\frac{y}{\langle\omega^2\rangle}\right), \tag{B 14}$$

$$P(\omega^2 = z) = \frac{1}{(2\pi)^{\frac{1}{2}}}\left(\frac{3}{\langle\omega^2\rangle}\right)^{\frac{3}{2}} z^{\frac{1}{2}} \exp\left(-\frac{3}{2}\frac{z}{\langle\omega^2\rangle}\right). \tag{B 15}$$

The averages coincide: $\langle y\rangle = \langle z\rangle = \langle\omega^2\rangle$.

For comparison we also present the PDF of $(\partial u_1/\partial x_1)^2$:

$$P\left(t = \frac{15}{2}\left(\frac{\partial u_1}{\partial x_1}\right)^2\right) = (2\pi\langle\omega^2\rangle)^{-\frac{1}{2}}(4t)^{-\frac{1}{2}} \exp\left\{-\frac{1}{2}\frac{t}{\langle\omega^2\rangle}\right\}. \tag{B 16}$$

The distribution of $\cos\gamma$, where γ is the angle between vorticity ω_i and the vector $S_{ik}\omega_k$ can be calculated directly from the integral

$$P(x = \cos\gamma) = \int \delta(x - \cos\gamma) P_3(\omega)\, \mathrm{d}^3\omega P_5(s)\, \mathrm{d}^5 s. \tag{B 17a}$$

Owing to the absence of correlation between ω_i and S_{ij} it is possible to direct the z-axis of the frame of reference along $\boldsymbol{\omega}$ when integrating over variables s_i. Then the vector $S_{ik}\omega_k$ has components $|\boldsymbol{\omega}|(S_{13}, S_{23}, S_{33})$ or in terms of variables s_i:

$$\omega_i S_{ij} = (|\boldsymbol{\omega}|)\left(s_2, s_1, -\frac{2}{\sqrt{3})\, s_5}\right),$$

so that

$$\cos\gamma = -\frac{2}{\sqrt{3}} s_5 (s_1^2 + s_2^2 + \tfrac{4}{3} s_5^2)^{-\frac{1}{2}}. \tag{B 17b}$$

Integration of (B 17) can be performed over s_3, s_4 and all ω using (B 11) and (B 12). Introducing the spherical coordinates

$$s_1 = r\sin\theta\cos\phi, \quad s_2 = r\sin\theta\sin\phi, \quad s_5 = r\cos\theta$$

and integrating one obtains

$$P(\cos\gamma = x) = 2\sqrt{3}(4-x^2)^{-\frac{3}{2}}. \tag{B 18}$$

It is noteworthy that by virtue of the nonlinear structure of $\cos\gamma$ in (B 17*b*) the PDF (B 17) is not constant even in absence of correlation between S_{ij} and ω_i.

The PDF of enstrophy generation term $\Omega = \omega_i S_{ik} \omega_k$ can be represented only in integral form. It is defined as

$$P\left(-\frac{2}{\sqrt{3}} s_5 \omega^2 = \Omega\right) = \int \delta\left(\Omega + \frac{2}{\sqrt{3}} s_5 \omega^2\right) P_3(\omega)\, \mathrm{d}^3\omega P_5(s)\, \mathrm{d}^5 s.$$

After integrating over all s_i (over s_5 with the help of a δ-function) and space angles in ω-space this PDF can be reduced to the integral

$$P(\Omega) = \frac{3^2 5^{\frac{1}{2}}}{2\pi \langle\omega^2\rangle^2} \int_0^\infty \mathrm{d}\omega \exp\left\{-\frac{3}{2}\frac{\omega^2}{\langle\omega^2\rangle} - \frac{15}{8}\frac{\Omega^2}{\langle\omega^2\rangle\,\omega^4}\right\}. \tag{B 19}$$

REFERENCES

Aref, H. 1990 Chaotic fluid dynamics and turbulent flow. In *Whither Turbulence? Turbulence at the Crossroads* (ed. J. Lumley), pp. 258–268. Springer.

Ashurst, W. T., Chen, J. Y. & Rogers, M. M. 1987*a* Pressure gradient alignment with strain rate and scalar gradient in simulated Navier–Stokes turbulence. *Phys. Fluids* **30**, 3293–3294.

Ashurst, W. T., Kerstein, A. R., Kerr, R. M. & Gibson, G. H 1987*b* Alignment of vorticity and scalar gradient with strain rate in simulated Navier Stokes Turbulence. *Phys. Fluids* **30**, 2343–2353.

Chen, H., Herring, J. R., Kerr, R. & Kraichnan, R. H. 1989 Non-Gaussian statistics in isotropic turbulence. *Phys. Fluids* A **1**, 1844–1854.

Frisch, U. & Orszag, S. A. 1990 Turbulence: Challenges for theory and experiment. *Phys. Today* **43**, 24–32.

Fung, J. C. H., Hunt, J. C. R., Malik, N. A. & Perkins, R. J. 1992 Kinematic simulation of homogeneous turbulence generated by unsteady random Fourier modes. *J. Fluid Mech.* **236**, 281–318.

Gagne, Y. 1991 Properties of fine scales in high Reynolds number turbulence. In *Advances in Turbulence 3* (ed. A. V. Johansson & P. H. Alfredsson) pp. 22–23. Springer.

George, W. K. 1990 The nature of turbulence. In *Forum on Turbulence Flows* (ed. W. M. Bower, M. J. Norris & M. Samimy), *ASME FED*, vol. 94, pp. 1–11.

Herring, J. R. & Kerr, R. M. 1989 Numerical simulation of turbulence. In *Theoretical and Applied Mechanics* (ed. P. Germain, M. Piau & D. Caillerie), pp. 101–116. North Holland.

Herring, J. R. & Métais, O. 1989 Numerical experiments in forced stably stratified turbulence. *J. Fluid Mech.* **202**, 97–115.

Hosokawa, I. 1990 Turbulence models and probability distribution and relevant quantities in isotropic turbulence. *Phys. Rev. Lett.* **66**, 1054–1057.

Kraichnan, R. H. & Panda, R. 1988 Depression of nonlinearity in decaying isotropic turbulence. *Phys. Fluids* **31**, 2395–2397.

LANDAU, L. D. & LIFSHITZ, E. M. 1987 *Fluid Mechanics*, 2nd edn. Pergamon.

MONIN, A. S. 1986 Hydrodynamic stability. *Soviet Phys. Usp.* **29**, 843–868.

MURAKAMI, Y., SHTILMAN, L. & LEVICH, E. 1992 Reducing turbulence by phase juggling, *Phys. Fluids* A **4**, 1776–1781.

NARASIMHA, R. 1990 The utility and drawbacks of traditional approaches. In *Whither turbulence? Turbulence at the Crossroads* (ed. J. L. Lumley), pp. 13–48. Springer.

POLIFKE, W. 1991 Statistics of helicity fluctuations in homogeneous turbulence. *Phys. Fluids* A **3**, 115–129.

POLIFKE, W. & SHTILMAN, L. 1989 The dynamics of helical decaying turbulence. *Phys. Fluids* A **1**, 2025–2033.

SHE, Z. S., JACKSON, E. & ORSZAG, S. A. 1990 Vortex structure and dynamics of turbulence. *Comput. Math. Appl. Mech. Engng* **80**, 173–183.

SHTILMAN, L., PELZ, R. & TSINOBER, A. 1988 Numerical investigation of helicity in turbulent flows. *Computers and Fluids* **16**, 341–347.

SHTILMAN, L. & POLIFKE, W. 1989 On the mechanism of the reduction of non-linearity. *Phys. Fluids* A **1**, 778–780.

SREENIVASAN, K. R. 1991 Fractals and multifractals in fluid turbulence. *Ann. Rev. Fluid Mech.* **23**, 539–600.

TSINOBER, A. 1990 On one property of Lamb vector in isotropic turbulent flows. *Phys. Fluid* A **2**, 484–486.

TSINOBER, A., KIT, E. & DRACOS, T. 1991 Measuring (frame independent) quantities composed of velocity derivatives in turbulent flows. In *Advances in Turbulence 3* (ed. A. V. Johansson & P. H. Alfredsson) pp. 514–523. Springer.

TSINOBER, A., KIT, E. & DRACOS, T. 1992 Experimental investigation of the field of velocity gradients in turbulent flows. *J. Fluid Mech.* **242**, 169–192.

VINCENT, A. & MENEGUZZI, M. 1991 The spatial structure and statistical properties of homogeneous turbulence. *J. Fluid Mech.* **225**, 1–20.